Equivalent-circuit, scaling, random-walk simulation, and an experimental study of self-similar fractal electrodes and interfaces

B. Sapoval and R. Gutfraind
Laboratoire de Physique de la Matière Condensée, Ecole Polytechnique, 91128 Palaiseau, France

P. Meakin
Department of Physics, University of Oslo, Blindern, 0316 Oslo 3, Norway

M. Keddam and H. Takenouti
Laboratoire de Physique des Liquides et Electrochimie, Université Pierre et Marie Curie 4, place Jussieu, 75252 Paris CEDEX 05, France

(Received 11 March 1993)

A comprehensive study of the macroscopic transport parameters of self-similar interfaces is presented. The iteration of a simplified equivalent leads to the prediction of a simple mathematical expression for the impedance of fractal electrodes in $d=2$ and 3 dimensions. The same value is predicted by scaling arguments and verified by extended numerical simulations in $d=2$. Experiments on model electrodes confirm the theoretical prediction. We introduce the approximate concept of an information fractal. It gives a very simple access to the theory and a description of the regions of the fractal surface which are really active for the transport. The same result should apply to transport across fractal membranes and to certain Eley-Rideal heterogeneous catalysis processes.

INTRODUCTION

Transport across rough or porous surfaces is a basic problem in the study of several natural or industrial processes. For instance, in the design of high-current batteries it is natural to consider porous electrodes as a means of increasing the net output current. Any process that is limited by transport across a surface or interface can be enhanced in this way. This is probably one of the reasons why in nature many systems such as plant roots, villi in the human intestine, or lung alveoli are found that have a ramified geometry that can be considered as approximate examples of large-area "fractal" structures [1–3]. In the case of a membrane, neutral reacting species are brought to the surface by diffusion currents instead of electrical currents and the transport across the membrane plays the same role as the redox reaction on the electrode [4]. The same type of problem may appear in heterogeneous chemical reactions or in the Eley-Rideal mechanism of heterogeneous catalysis [5,6]. In the last case molecules have to diffuse before reacting on irregular surfaces.

The problem is best stated in the electrochemical frame because frequency-dependent transport can easily be studied experimentally by impedance spectroscopy. A variety of experimental studies have indicated that most often the impedance of electrochemical cells behave as

$$Z=R_0+k(j\omega)^{-\eta}\ . \tag{1}$$

R_0 represents the electrolyte resistance, ω is the frequency of the ac applied voltage, and $j=(-1)^{1/2}$. This behavior is called "constant-phase-angle" (CPA) response and η is the CPA exponent which depends on surface electrode roughness (k is a constant) [7,8].

There have been essentially two approaches to aid in understanding this phenomenon, an old problem in electrochemistry [9]. First, it can be attributed to a particular distribution of microscopic transport parameters on a planar surface [10]. Second, it can be related to the electrode surface geometry. (Both phenomena can occur simultaneously in experiments.) The understanding of the influence of the surface geometry on the net transport is the general problem to which this paper is devoted. In recent years, experimental and theoretical works have been focused on the relationship between fractal geometry and the CPA exponent [5,11–31]. Both self-similar and self-affine fractal surfaces have been explored with the objective of determining if the CPA exponent η of Eq. (1) is related to the dimensionality D or Hurst exponent H. A more ambitious objective is to provide an algebraic expression for the impedance that can be used to compare the performance of fractal interfaces with nonfractal ones. For fractal surfaces there exist exact algebraic results for the impedance only on specific model electrodes and no general conclusion can be drawn [13–15].

Recently it has been realized that an exact mapping exists between the response of an electrode under dc conditions and the net diffusion across a membrane of the same geometry [4,32]. In addition it can be shown, using linear-response theory, that a simple and direct connection exists between the ac and the dc response [15,32,33]. These equivalences were used to investigate the properties of both fractal and nonfractal electrodes (and related processes such as transport across membranes). Applying these ideas, Meakin and Sapoval have shown that for

1063-651X/93/48(5)/3333(12)/$06.00

a variety of self-similar ramified fractals in $d=2$, the constant-phase-angle exponent is related to the fractal dimensionality of the electrode surface D by

$$\eta = 1/D \tag{2}$$

for the case of electrodes embedded in a two-dimensional space [33]. This relationship between η and D is supported by a scaling argument based on the fact that the information dimension of the harmonic measure is 1 in $d=2$ [34]. Equation (2) was first proposed by Le Méhauté, but was supported by an erroneous gauge argument [11]. Nyikos and Pajkossy gave the same result based on dimensional analysis [or $\eta=1/(D-1)$ for electrodes embedded in $d=3$] [13]. However, Liu and co-workers and Sapoval, Chazalviel, and Peyrière gave exact counterexamples on specific model electrodes [12,14,15]. (This contradiction will be explained later.) Halsey and Liebig [23] and Ball [35] proposed recently a slightly different relation.

At the same time, a method based on an iteration calculation of a simplified equivalent circuit had been proposed by Keddam and Takenouti [24]. In its initial form, the equivalent circuit approach predicted that the CPA exponent η was not a function of the fractal dimension D of the electrode and accordingly, preliminary low-frequency experiments seemed to contradict relation (2). (The early experiments of Nyikos and Pajkossy were performed at high frequency on model electrodes of large size, a situation in which impedance measurements can be perturbed by the effect of parasitic capacitances.) In order to clear this contradiction we have undertaken a joint effort including a more complete set of simulations and experiments which now give compatible results. We also present an equivalent circuit approach together with a crossover argument from which we are able to predict that η follows relation (2), but also predicts an algebraic expression for the impedance. This simplified approach permits us to obtain an algebraic formula which is very well verified by the diffusion simulations. The compatibility between the experiments and both theoretical approaches provides a complete result on the fractal electrode problem in $d=2$, at least for self-similar ramified electrodes.

ITERATED EQUIVALENT CIRCUIT IN $d=2$

The purpose of this section is to show that an equivalent circuit approach permits a simple description of this problem. The simple approximate calculation that we describe predicts an impedance that will be verified by the numerical simulations discussed in the next section.

We start with the smallest element of the two-dimensional (2D) fractal electrode. It is supposed to be a linear piece of metal of length l and thickness b. It is a capacitor with impedance

$$Z_0=(j\gamma\omega lb)^{-1}, \tag{3}$$

where γ is the specific capacitance of the interface. The fractal generator is made of a segment of length Pl, which is cut in P equal parts of length l, of which N are kept and M identical segments are added. The electrode is

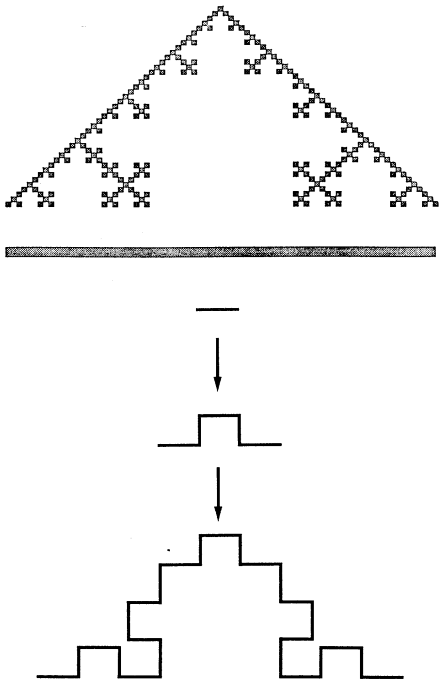

FIG. 1. Deterministic fractal electrode. Here $N=2$, $M=3$, $P=3$, and $D=\log_{10}(5)/\log_{10}(3)$. Top, geometry of the experimental cell; bottom, construction of the fractal electrode.

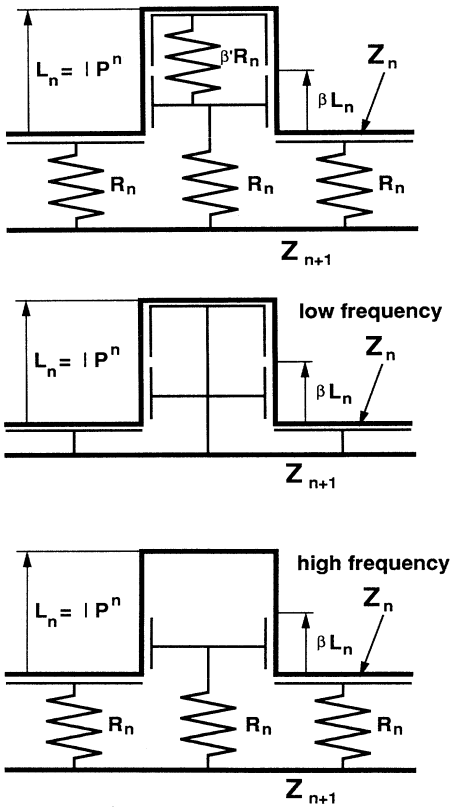

FIG. 2. Equivalent circuit used to approximate the problem. Top, the circuit; middle, the low-frequency approximation; bottom, the high-frequency approximation.

built by iteration as in Fig. 1. The "front" part is N reproductions of the initial smaller parts and M equivalent parts are added. The fractal dimension is

$$D=\ln(M+N)/\ln(P) , \tag{4}$$

where P is the dilatation factor. We can imagine building the electrochemical cell by constructing the fractal by iteration from the smaller element. At stage $n+1$ the impedance Z_{n+1} of the larger unit can be represented in terms of the impedance Z_n of the cell at stage n using the equivalent circuit shown in Fig. 2 (top), which has an impedance given by

$$\frac{1}{Z_{n+1}}=\frac{N}{Z_n+R_n}+\frac{P-N}{R_n+\dfrac{1}{\dfrac{2\beta}{Z_n}+\dfrac{1}{\beta' R_n+\dfrac{Z_n}{M/(P-N)-2\beta}}}} . \tag{5}$$

The numerical factors β and β' are to be discussed later. The impedance of the real cell is then a finite continued fraction. This formula is apparently complex, but we will only use the low-frequency and the high-frequency approximations which are represented by the very simple circuits shown in the middle and bottom of Fig. 2.

From one stage to the next the electrolyte cell varies in size but its resistance R_n remains constant. The electrolyte resistance R_n are squares of side l, Pl, $P^2 l$, . . . and thickness b. For an electrolyte of resistivity ρ, the resistance at the first stage is

$$R_0=\rho l/lb=\rho/b \tag{6}$$

and $R_n=R_{n-1}=\cdots=R_0$ in $d=2$. It is convenient to study the recursion (5) using the reduced variable $z_n=Z_n/R_n$:

$$\frac{1}{z_{n+1}}=\frac{N}{z_n+1}+\frac{P-N}{1+\dfrac{1}{\dfrac{2\beta}{z_n}+\dfrac{1}{\beta'+\dfrac{z_n}{M/(P-N)-2\beta}}}} . \tag{7}$$

The reduced variable z_0 has a modulus equal to

$$|z_0|=(\rho\gamma\omega l)^{-1}=\Lambda/l , \tag{8}$$

where $\Lambda=(\rho\gamma\omega)^{-1}$ is the scale length in the problem [15]. We work at frequencies such that

$$\Lambda/l=|z_0|\gg 1 \tag{9}$$

and for the first stages of iteration (7) reduces to

$$z_{n+1}\approx z_n/(N+M) . \tag{10}$$

Whatever the values of β and β' the same dependence is obtained because in this regime the cell impedance is essentially that of the surface capacitance. The iteration can proceed this way up to a critical value $n=\nu(\omega)$ for which $z_{\nu(\omega)}$ is of the order of 1

$$z_{\nu(\omega)}\approx z_0(N+M)^{-\nu(\omega)}\approx 1 . \tag{11}$$

The critical value $\nu(\omega)$ is

$$\nu(\omega)\approx\ln|z_0|/\ln(N+M) =\ln(\Lambda/l)/\ln(N+M) . \tag{12}$$

After the stage $\nu(\omega)$ we reach a regime where $z_n<1$ and the iteration procedure (7) cannot be performed simply. In this case the impedance of the electrode becomes much smaller than the impedance of the electrolyte. This is a situation in which the distribution of potential lines is determined by the usual harmonic potential distribution in the same geometry (the electric potential is the solution of Laplace equation with the boundary condition that the potential is zero everywhere on the surface of the electrode of interest). We write

$$z_n=z_{n,\text{yte}}+z_{n,\text{ode}} , \tag{13}$$

where $z_{n,\text{yte}}$ and $z_{n,\text{ode}}$ represent the electrolyte and the electrode contributions, respectively. If we look for $z_{n,\text{yte}}$ for n large enough, the contribution of the electrode in the recursion can be neglected. In this situation we know that the electrolyte resistance must be independent of the order of iteration (in $d=2$) because the cell geometry remains similar from one stage to the next. This is an important constraint, which implies that (7) can be approximated in this regime by

$$z_{n+1}\approx(1+z_n)/P . \tag{14}$$

This approximation implies that in Eq. (7) β must be equal to $\frac{1}{2}$ and that β' is large enough so that the influence of the geometrical irregularity on the current in the total electrochemical cell can be neglected as a first approximation. This is qualitatively justified by the shape of the equipotentials near the electrode as they have been computed by Evertsz and Mandelbrot in the same geometry (see Fig. 3) [36]. The limiting value for the resistance of the electrolyte is obtained by setting $z_{n+1,\text{yte}}=z_{n,\text{yte}}$ in the previous relation, or

$$z_{n=\infty,\text{yte}}\approx(P-1)^{-1} . \tag{15}$$

But if β is equal to $\frac{1}{2}$ and β' is large, then relation (14), being a good approximation of (7), can be applied to the total impedance (13). The recursion relation for the elec-

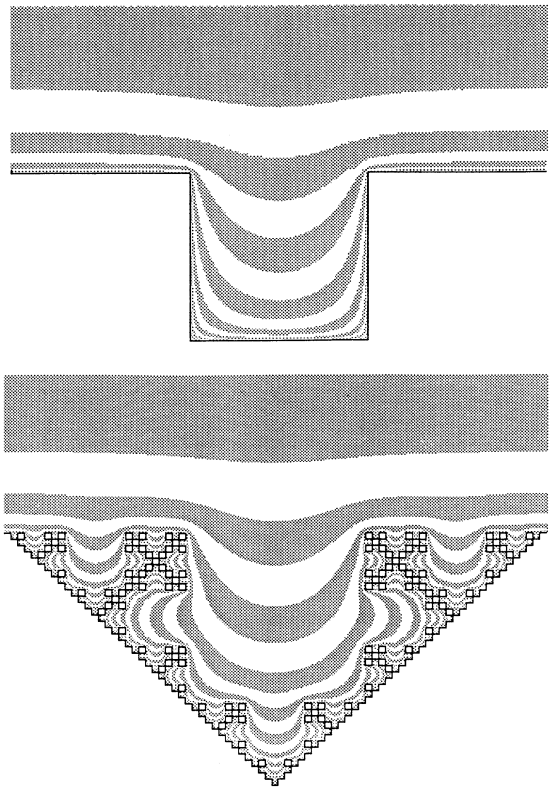

FIG. 3. Potential distribution for generation 1 and 4 of the fractal electrode. (From Evertsz and Mandelbrot [36]; see Ref. [38]). In this "zebra" representation the potential varies by a factor of 2 from one separation line to the next. Whatever the generation, the equipotential lines near the entrance of the pore are only slightly perturbed by the existence of smaller pores. Our approximation amounts to supposing that the equipotential lines are flat at the entrance of each pore.

trode contribution is obtained by inserting

$$z_n=(P-1)^{-1}+z_{n,\mathrm{ode}} \tag{16}$$

in relation (14) to give

$$z_{n+1,\mathrm{ode}}=z_{n,\mathrm{ode}}/P \ . \tag{17}$$

This is a remarkable result because it tells us that the electrode contribution is inversely proportional to the size of the electrode, which increases by a factor P at each iteration. It is a direct consequence of the invariance of the electrolyte resistance when the cell is dilatated. For an electrode of size L the iteration must be performed $n(L)$ times such that the electrode size L is given by

$$L=lP^{n(L)} \tag{18}$$

or

$$n(L)=\ln(L/l)/\ln P \ . \tag{19}$$

From (17) the electrode impedance is given by

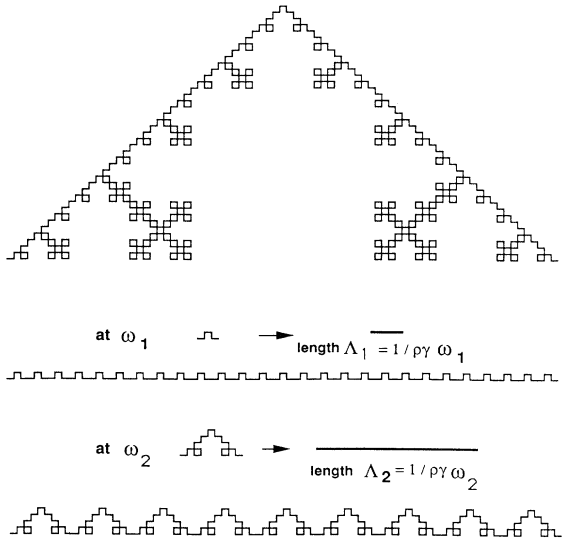

FIG. 4. An equivalent representation of the result. Note that the length of the effective working surface varies with frequency.

$$\begin{aligned} z_{n(L),\mathrm{ode}} &\approx p^{-n(L)+\nu(\omega)} z_{\nu(\omega),\mathrm{ode}} \\ &\approx p^{-n(L)+\nu(\omega)}(N+M)^{-\nu(\omega)} z_0 \ . \end{aligned} \tag{20}$$

Two asymptotic regimes have been defined. The first one, obtained for $n(L)\ll\nu(\omega)$, corresponds to sufficiently small object sizes. In this regime the cell impedance is dominated by the surface impedance. The second asymptotic regime $n(L)\gg\nu(\omega)$ corresponds to large objects, where the impedance of the cell is dominated by the electrolyte.

Substitution of (6), (8), (12), and (19) in (20) gives the admittance of the electrode

$$Y(L)\approx Lb\rho^{\eta-1}(j\gamma\omega)^{\eta} l^{\eta-1} \tag{21}$$

with $\eta=1/D$. There is a very simple way, illustrated in Fig. 4, to describe this result. At a frequency ω the electrode admittance can be considered to be given by the admittance $R_0^{-1}=b/\rho$ multiplied by a number $L/L_c(\omega)$ of equivalent regions where $L_c(\omega)=lP^{\nu(\omega)}$ is the size at crossover. The size at the crossover is the size of the electrode for which the surface impedance is equal to the access resistance. It is given by

$$L_c(\omega)=l(\Lambda/l)^{1/D} \tag{22}$$

and again formula (21) is obtained.

A CROSSOVER ARGUMENT TO OBTAIN THE ADMITTANCE IN $d=2$: THE NOTION OF AN INFORMATION FRACTAL

For a given electrode, if the frequency is small enough, the response will be purely capacitive because $n(L)<\nu(\omega)$. The admittance is capacitive and

$$Y=lb(L/l)^{D}\gamma\omega \ . \tag{23}$$

On the contrary if $n(L) > \nu(\omega)$ and if the admittance is of the CPA type, dimensional analysis imposes that $Y \sim (\text{length})^{1+\eta} \rho^{\eta-1} (\gamma\omega)^{\eta}$. For a real 2D cell of thickness b the admittance is proportional to b so that the expression of the admittance must be $Y \sim b(\text{length})^{\eta} \rho^{\eta-1} (\gamma\omega)^{\eta}$.

If we now postulate that the admittance is a linear function of the macroscopic size of the electrode L, we can write

$$Y \sim Lb\rho^{\eta-1} (\gamma\omega)^{\eta} (l)^{\eta-1} \tag{24}$$

because the only other length in the fractal is the smallest feature size (or lower cutoff) l.

The crossover frequency ω_c between the purely capacitive and purely CPA regime is obtained when $n(L) = \nu(\omega)$ at a frequency ω_c given by Eqs. (12) and (18)

$$\omega_c \sim (\rho\gamma l)^{-1} (L/l)^{-D} . \tag{25}$$

At the crossover frequency (25) both expressions (23) and (24) must be equal and by equating the exponents of L the result $\eta = 1/D$ is obtained. The crucial hypothesis is the linear dependence of the electrode admittance on the size L. This is itself a consequence of Eq. (14), which follows from the fact that in $d = 2$ the limit admittance of the cell is that of the electrolyte which must be independent of the order of iteration.

Using the high-frequency approximation, it is possible to construct directly the set on which the current is really absorbed. This is shown in Fig. 5. At the top the thin line can be considered as the generator of the set on which the current arrives on the electrode. It is the generator of a fractal object which can be called the "information fractal" of the corresponding electrode [37]. The information fractal is shown in Fig. 5. Its fractal dimension is exactly one which means that when measured with a ruler $\mathcal{L}$ a number of rulers $L/\mathcal{L}$ must be found. When measured with a ruler $L_c(\omega)$ or larger, a number of rulers $L/L_c(\omega)$ are found. In the regime of interest l is smaller than $L_c(\omega)$. At the bottom of Fig. 5 we have represented the zones that are effectively reached by the current at a frequency where $L_c(\omega)$ is the smallest element of the information fractal. The current reaches equally all the elements of the structure of size smaller than $L_c(\omega)$, that is, those which are under the thick line. In that sense the working region has a dimension equal to D for rulers smaller than $L_c(\omega)$ and a dimension $D_I = 1$ for rulers larger than $L_c(\omega)$. At a given frequency, the geometry of the information fractal describes the working region of the electrode. In a pure diffusion problem it would describe the working part of a membrane or of a catalyst. Note that this notion of active information set can be extended to arbitrary geometries [38].

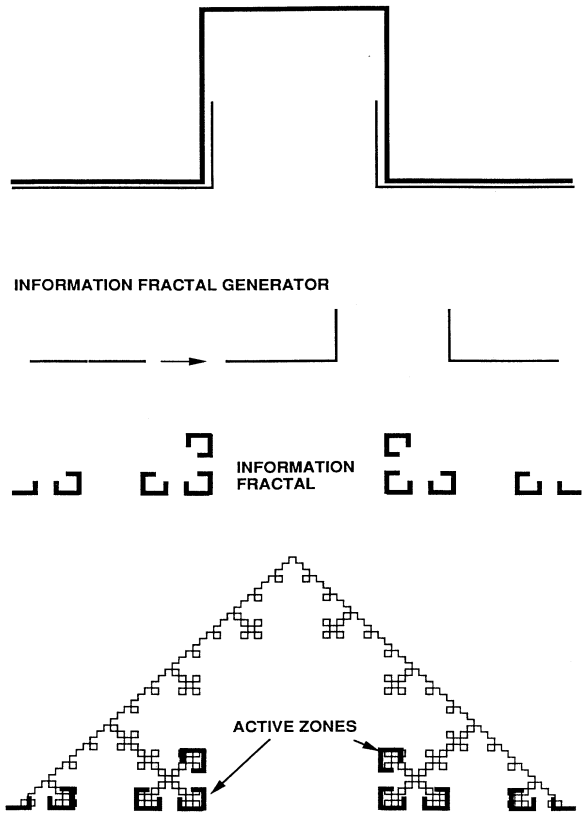

FIG. 5. Definition of the information fractal. At the top the approximation of the working part of the fractal generator is shown. This defines the generator of the information fractal, which is built as shown. The information fractal indicates the regions of the electrode that are really working at a frequency ω. These regions are indicated by the thick line. Correspondingly they would also be the working regions of a membrane or a catalyst with the corresponding values of σ.

COMPUTER SIMULATIONS

We consider here the electrochemical cell shown in Fig. 1(a) and we compute its response by numerical simulations. The theoretical approach and the numerical algorithm that we use are based on the exact analogy between the electrochemical problem and a diffusion problem in the same geometry [4,5,32]. They are described in detail in Ref. [33]. We recall briefly the numerical procedure.

In the simulation random walkers are launched, one at a time, from a randomly selected lattice site on the counter electrode at $y = 1$. The random walker is then allowed to execute a random-walk trajectory taking on lattice steps of length 1 near either of the electrodes and longer off-lattice steps when it is far from either electrode. As in Ref. [33] the lengths of the long off-lattice steps are restricted so that the random walker cannot reach either electrode in a single step. We used periodic boundary conditions in the lateral (x) direction. If the random walker reaches the flat electrode from which it was launched, the random walk is terminated and a new random walk is launched from a randomly selected (lateral) position at $y = 1$. If the random walker attempts to step onto an occupied site associated with the porous electrode, it is absorbed with probability σ (the sticking probability) or returned to the unoccupied site that it previously occupied with probability $1 - \sigma$. If the random

walker is absorbed, a record is kept of the absorption event and the random walk is terminated. In a real diffusion situation most of the particles which leave the diffusion source return to it. This is due to the fact that the net flux, from Fick's law, is proportional to the gradient of the concentration and not to the concentration itself. The net flux is due to the very few particles that are absorbed before returning to the source. We then want to find the probability p_a of absorption of a particle by the working membrane. The basic quantity that can be measured in these simulations is the average number $\langle N_r \rangle$ of random walkers that return to the smooth electrode before a random walker is absorbed by the porous electrode. The probability of absorption p_a is the inverse of $\langle N_r \rangle$. If N_s is the number of sites on the diffusion source (external electrode), p_0 the occupation probability of a site at the source, and $1/\tau$ the jump probability per unit time, the number of particles which are launched per unit time is $p_0 N_s/4\tau$. The steady-state flux Φ is the product of that number by the effective absorption probability p_a and

$$\Phi=(p_0 N_s/4\tau)p_a \ . \tag{26}$$

The concentration is related to the occupation probability p and lattice spacing a by

$$c=p/a^2 \tag{27}$$

and the diffusion admittance Y is defined by $\Phi=Y_D c_0$, where c_0 is the concentration at the source. Then

$$Y_D=N_s(a^2/4\tau)\langle N_r \rangle^{-1} \tag{28}$$

with $N_s=(L/a)=(L/l)(l/a)$. The admittance computed this way corresponds to that of the total electrochemical cell. The electrode contribution must be found by using in relation (28) a value of $\langle N_r \rangle=\langle N_r(\sigma) \rangle - \langle N_r(\sigma=1) \rangle$ to subtract the electrolyte resistance contribution [33]. The estimate becomes more accurate as the results from more random-walk trajectories are averaged. In most of our simulations the procedure described above was continued until 15 000–20 000 random walkers had been absorbed by the porous electrode. In these simulations the dependence of $\langle N_r \rangle$ on σ was determined using 17 different values for σ ($\sigma=2^{-n}$, $n=0$–16).

The results are shown in Figs. 6–9. In Fig. 6 a random trajectory is shown for a sticking probability of 10^{-3} and for three different values of the lattice spacing: from top to bottom the smallest element of the fractal electrode l is equal respectively to a, $2a$, and $4a$. The numerical results of the impedance calculation are given in Fig. 7 for $l=a$, $2a, 4a, \ldots, 64a$. Apart from a small region corresponding to the very large values of σ, a CPA behavior is found, followed by a crossover to a capacitive behavior for very low values of σ. The fact that the large σ region does not show CPA behavior corresponds to the fact that the random walkers do not explore the fractal geometry but the linear geometry of the smaller cutoff length l. Also in that region the electrode contribution is very small and the numerical uncertainty is comparatively larger.

In order to compare quantitatively the simulation with the algebraic expression (21) we first discuss (21) in terms of diffusion parameters. In the physical world, there exist two basic physical quantities: the diffusion coefficient D (which corresponds to ρ^{-1}) and the coefficient of trans-

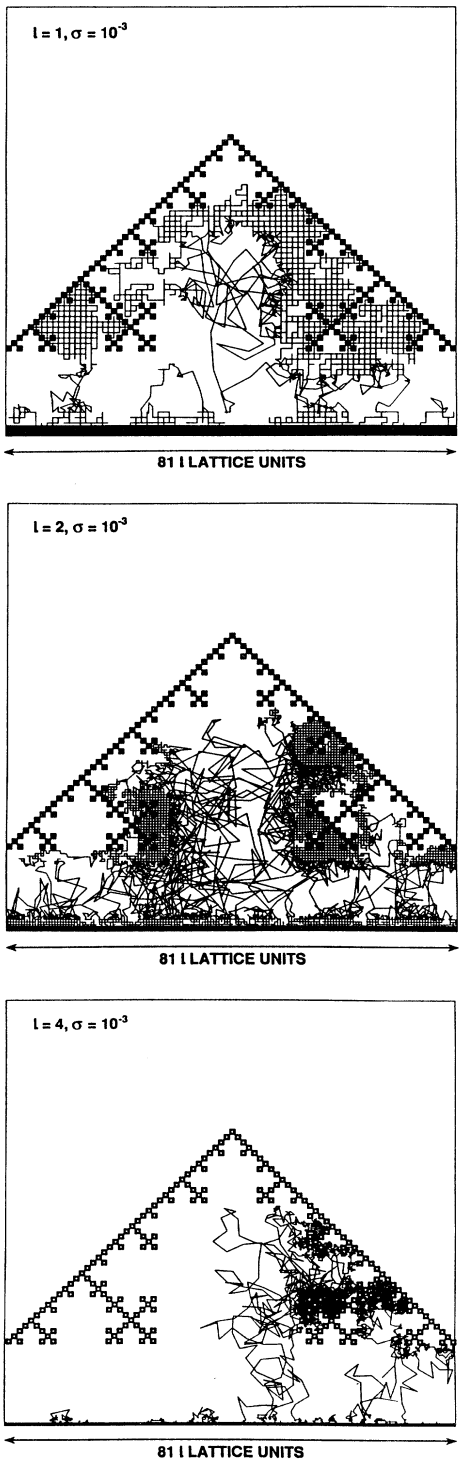

FIG. 6. A random walk trajectory for smaller and smaller lattice spacing. Far from the surface of the fractal, long, off-lattice steps are taken.

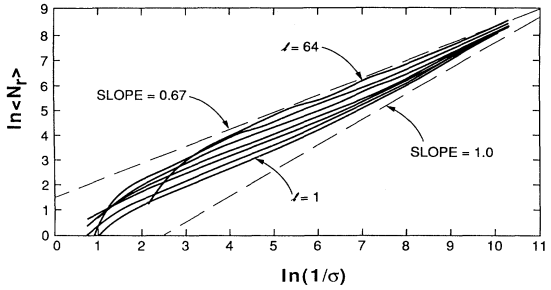

FIG. 7. Results of the numerical simulations for the geometry of Fig. 1.

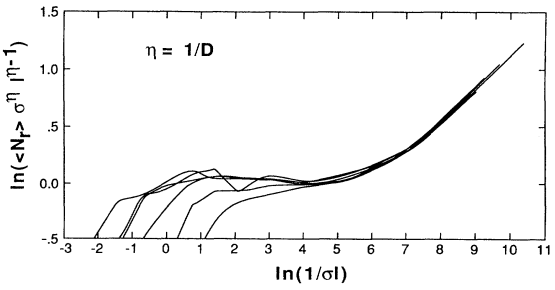

FIG. 9. Data collapse plot of the capacitive regime using Eq. (35).

port across the surface (permeability) W (which corresponds to $\gamma\omega$). (If c is the concentration at the surface of a linear membrane of length L, the net flux across the membrane is cWL.) On a square lattice

$$D=a^2/4\tau\ , \tag{29}$$

$$W=a\sigma/4\tau\ . \tag{30}$$

The sticking probability σ is not determined uniquely from D and W but depends on the lattice spacing. The true physical variable in that problem is the length [15,33]

$$\Lambda=D/W=a/\sigma\ . \tag{31}$$

If D is substituted for ρ^{-1} and W is substituted for $j\gamma\omega$ in (21) the result $Y_D=ALbD^{1-\eta}W^{\eta}l^{\eta-1}$ is obtained. We have introduced a numerical factor A to take into account that relations (21) and (24) are proportionality relations. For the $d=2$ system in which the simulation is performed, the value of b is $b=1$ so that the formula that must be tested is

$$Y_D=ALD^{1-\eta}W^{\eta}l^{\eta-1} \tag{32}$$

and from (26–29) we predict that

$$\langle N_r\rangle=A^{-1}a^{\eta-1}\sigma^{-\eta}l^{1-\eta}\ . \tag{33}$$

Figure 8 shows a plot of $\langle N_r\rangle\sigma^{\eta}l^{\eta-1}$ (or supposedly A^{-1}) with $\eta=1/D=0.6826$ as a function of σ. A collapse of all the data for all the values of l on a single horizontal line is observed. In computer units $a=1$, so that in these units $\langle N_r\rangle\sigma^{\eta}l^{\eta-1}=A^{-1}=1$ within the simulation noise as verified in the figure.

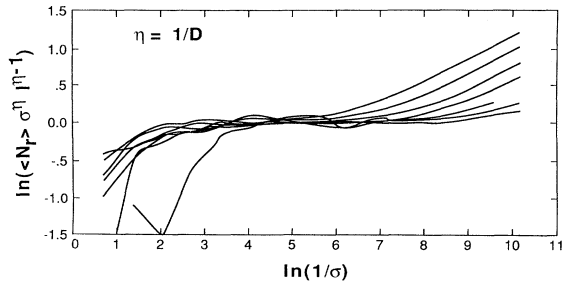

FIG. 8. Data collapse plot of the CPA regime using Eq. (33).

In the very small σ regime, $\eta=1$ and the admittance is given by the total length of the fractal and

$$Y=l(L/l)^D W\ . \tag{34}$$

Using Eqs. (27) and (29) the quantity $\langle N_r\rangle\sigma^{\eta}l^{\eta-1}$ is found to be equal to

$$\langle N_r\rangle\sigma^{\eta}l^{\eta-1}=(L/l)^{1-D}(1/\sigma l)^{1-\eta}\ . \tag{35}$$

Figure 9 shows the dependence of $\ln(\langle N_r\rangle\sigma^{\eta}l^{\eta-1})$ on $\ln(1/\sigma l)$. For systems in which L/l is constant, as in our case, a collapse of all the curves in the small σ regime is observed. The slope is measured to be approximately equal to 0.316 to be compared with the theoretical value $1-\eta=0.317$. A comparison of Eqs. (32) and (34) indicates a crossover between the CPA regime and the capacitive regime when

$$\Lambda/l=[L_c(\sigma)/l]^D\ , \tag{36}$$

if $A=1$ is verified to a good approximation by the simulations. The crossover distance $L_c(\sigma)$ corresponds to the crossover $L_c(\omega)$ but can be obtained directly from the diffusion equivalence. It corresponds to the Euclidian distance that a random walker that hits the electrode with absorption probability σ travels before being absorbed. The walk is terminated when the number of fractal sites within the Euclidian distance $L_c(\sigma)$ or $(l/a)[L_c(\sigma)/l]^D$ is equal to the average number of collisions before absorption $1/\sigma$. This equality gives (36) independently of the preceding discussion. Now, in the same spirit, if we consider a coarse graining of the object to the size $L_c(\sigma)$, the new sites can be considered as absorbing random walkers with probability 1. On the renormalized object, the fact that the information dimension D_I of the harmonic measure is exactly equal to 1 in $d=2$ implies that the probability of adsorption by the surface for random walkers that diffuse from the bulk is concentrated on a subset of dimension 1. This means that the size measured in renormalized sites of the regions where the new random walkers are absorbed is proportional to L and then that the admittance is proportional to L as postulated above.

On the lattice the value of Λ/l is $a/l\sigma$, so that for a fractal for which L/l is given, the crossover should be found for a value of $a/l\sigma$ equal to $(L/l)^D$ independently of l. This is what is observed in Fig. 9 in which the

numerical value of the crossover is shown to be of order 550. This value must be compared with $(L/l)^D=(81)^{\ln 5/\ln 3}=625.03\ldots$.

The overall conclusion of the simulations is a strong indication that Eq. (21) is really an exact result because the prefactor A is found equal to 1 within numerical uncertainty. It also confirms that the simulations in Ref. [31] were correct: the size of the inner cutoff length does not influence the CPA exponent and the cell geometry does not modify its value.

EXPERIMENTS

We first recall an already published determination of the equipotential line distribution for deterministic self-similar electrodes [24]. The experiment uses an ac potential probe to determine the equipotential line distribution in the cell. The results are shown for two different frequencies in Fig. 10. The equipotential distribution depends on the frequency through the surface impedance. The left-hand side of Fig. 10 (top) shows a distribution corresponding to the high-frequency side of the crossover. This is characterized by the approximately exponential decay of the voltage in the central pore. On the contrary, at 1 kHz the potential exhibits a more linear decay which corresponds to the distribution below the crossover (more precisely below the crossover, but very close to it). We did not repeat this experiment at lower frequency because it is rather tedius, but at still lower frequencies the effect should be even more pronounced. This is shown in the lower part of Fig. 10, which presents the results of Ref. [24] obtained with the canonical Koch electrode.

For practical reasons, the detailed impedance measurements were made using, as a working electrode, a Koch ($D=\ln 4/\ln 3=1.26\ldots$) profile with four levels of hierarchy built in a 1-mm-thick aluminum plate. Both sides of the aluminum sheet were covered with a heat curing varnish before machining. Then the fractal electrode was anodized at a very low current to form a uniform, a principle capacitive, oxide layer. The anodization is a very slow process which necessitates ionic transport through the already formed oxide layer, and the current is then uniformly distributed on the entire electrode surface (r is very large). The electrochemical cell is schematically described in Fig. 11. The electrolyte was an aqueous solution of Na_2SO_4 with concentration ranging from $10^{-3}M$ to $10^{-1}M$. The impedance measurements were performed at open circuit potential.

The electrolyte cell was a conventional three-electrode design: a fractal working electrode (WE), an aluminum ribbon used for the local potential probe [reference electrode (REF)], and an aluminum sheet as the counter electrode (CE). The potential between the reference and the working electrode was maintained constant by means of a Schlumberger Model EI1286 potentiostat. At this potential a small-amplitude perturbing signal ($\Delta U=10$ mV rms at frequency f) was superimposed for impedance measurements. The latter was carried out by a frequency-response analyzer (FRA) (Schlumberger Model FRA1250). A personal computer controlled all the measurements and experimental results for $Z(f)$ were stored in a data file.

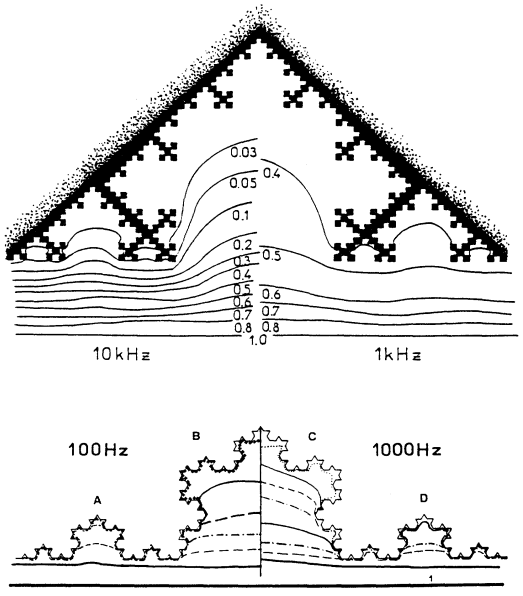

FIG. 10. Potential map for various electrodes and frequencies. Top, the electrode of Fig. 1; bottom, potential distribution for the Koch electrode. For the sake of clarity in this reduced picture the values of the intermediate potentials have not been written in the figure. The equipotential lines corresponds respectively to 0.9, 0.8, and 0.75 in the A region; 0.9, 0.8, . . . , 0.4 in the B region; 0.9, 0.8, 0.7, 0.5, 0.3, 0.2, 0.1, and 0.05 in the C region; and 0.9, 0.8, 0.7, and 0.5 in the D region.

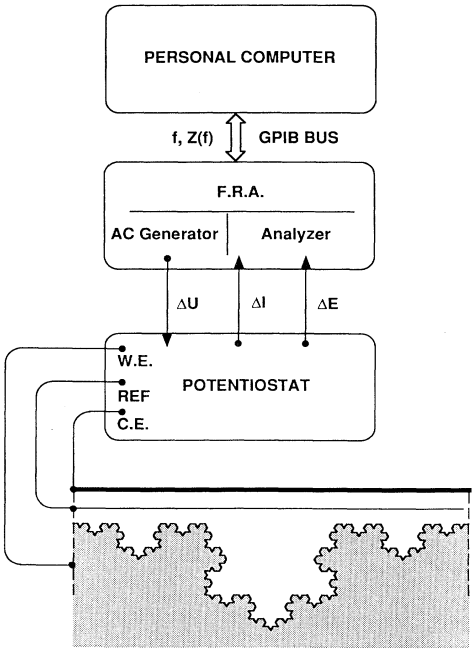

FIG. 11. Experimental setup for impedance measurement. GPIB denotes a general-purpose interface bus.

The results for the canonical Koch electrode are shown in Fig. 12. The imaginary part of the cell impedance is given for three electrolyte concentrations in the Bode plot. A Bode plot is a plot of the logarithm of the impedance, here of the imaginary part of the impedance, as a function of the logarithm of the frequency. Note that from relation (1), the imaginary part of the total cell impedance is related to the electrode contribution only. A CPA impedance is linear with slope $-\eta$ in the Bode representation.

In the experimental results for the Koch electrode two regions were observed. At low frequency there is a CPA behavior with an exponent η_0 smaller than 1. If the oxide covering the electrode behaved as a true insulator, the value of η_0 should be exactly equal to 1. This is not the case, but it is a common feature for oxydized electrodes attributable to anomalous transport through the oxide layer. In order to calibrate our results we have studied the response of macroscopically flat electrodes prepared under the same conditions, i.e., with the same current density and duration. The impedances spectrum of these flat electrode are shown in Fig. 13. The flat electrode also exhibits a CPA behavior and the above calculations have to be modified accordingly. Equations (3) and (8) must be replaced by $Z_0=\gamma'^{-1}(j\omega)^{-\eta_0}(lb)^{-1}$ and $|z_0|=(\rho\gamma' l)^{-1}\omega^{-\eta_0}=\Lambda'/l$ with $\Lambda'=(\rho\gamma')^{-1}\omega^{-\eta_0}$. The quantity that is really measured and plotted in Fig. 13 for a flat electrode of area S is $-\mathrm{Im}(Z)=\sin(\eta_0\pi/2)\gamma'^{-1}\omega^{-\eta_0}S^{-1}$ from which the values for η_0 and γ' can be obtained for the three electrolyte concentrations. From the data of Fig. 13 the results $\eta_0=0.74$ and $\gamma'=4.5\times10^{-6}$ for the $0.001M$ solution, $\eta_0=0.67$ and $\gamma'=4\times10^{-6}$ for the $0.01M$ solution, and $\eta_0=0.68$ and $\gamma'=3.8\times10^{-6}$ for the $0.1M$ solution were obtained.

At low frequency the impedance of the Koch electrode should be that of the total surface:

$$-\mathrm{Im}(Z)=\sin(\eta_0\pi/2)(\gamma' lb)^{-1}(l/L)^D\omega^{-\eta_0}. \quad (37)$$

Taking care of the CPA behavior of the flat electrode we can easily write the equivalent of Eq. (21) in the fractal regime and predict

$$-\mathrm{Im}(Z)\approx\sin(\eta_0\pi/2D)(\rho l/Lb)(\rho l\gamma')^{-1/D}\omega^{-\eta_0/D}. \quad (38)$$

We may now compare the first-principle predictions (37) and (38) with experiment using the values of γ' and η_0 calibrated with the flat electrode, the geometrical parameters of the electrodes ($l=0.3$ cm, and $L=3^4 l=24.3$ cm), and the electrolyte resistivities $\rho_{0.1M}=68\ \Omega$ cm, $\rho_{0.01M}=680\ \Omega$ cm, and $\rho_{0.001M}=6.8$ kΩ cm. These predictions are shown by the lines in Fig. 12. There is an overall compatibility between theory and experiment. Considering that there are no adjustable parameters, this

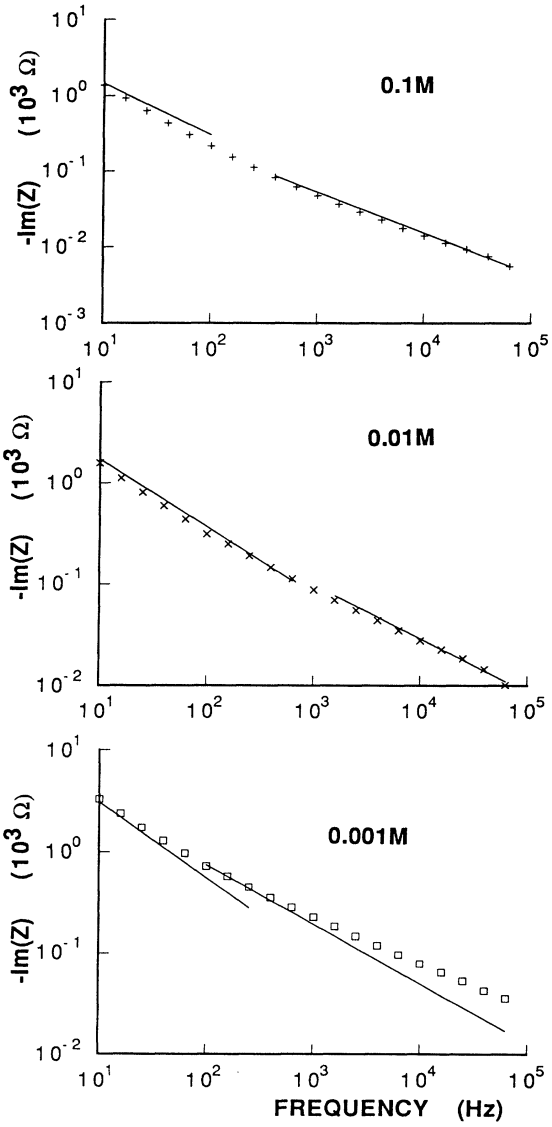

FIG. 12. Bode plot of the impedance of Koch electrodes for several electrolyte concentrations: $0.1M$, $0.01M$, and $0.001M$. Im(Z) stands for the imaginary part of Z as defined in the text.

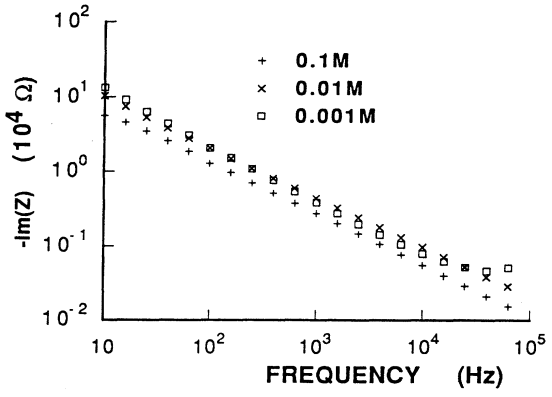

FIG. 13. Bode plot of the impedance of planar electrodes for several electrolyte concentrations: $0.1M$, $0.01M$, and $0.001M$. The planar electrode presents itself a CPA behavior with an exponent η_0. The high-frequency anomaly is an experimental artifact due to the method of measurement.

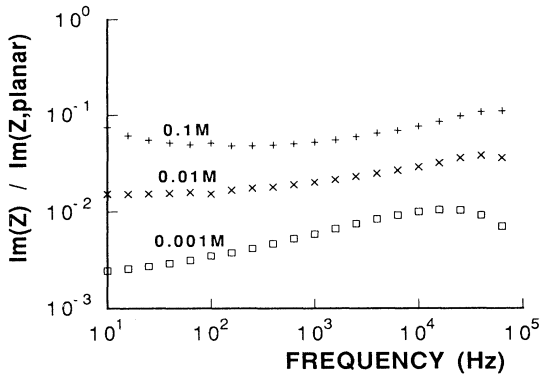

FIG. 14. Bode plot of the ratio of the impedance of the fractal electrode to the impedance of the planar electrode. The curves have been arbitrarily translated for clarity.

set of experiments can be considered as a fair confirmation of the theoretical approaches discussed above. In this frame, we consider that the experimental results are compatible with relation (2), but cannot be considered as a proof of this relation.

The fact that there still exist small discrepancies between theory and experiment as apparent in Fig. 12 can probably be related to a more complex behavior of the flat interface itself or to the fact that the oxide is not really distributed uniformly on the fractal electrode. To illustrate this point (and the difficulty in general of these determinations) we give in Fig. 14 the Bode plot of the ratio Im (Z_{fractal})/Im (Z_{flat}). At low frequency it should present a horizontal line up to the crossover frequency. Above the crossover it should be linear with a slope of $-\eta_0\eta_{\text{CPA}}+\eta_0=\eta_0(1-\eta_{\text{CPA}})$. The real behavior is not as simple as that. This may be due to the fact that the crossover is not sharp or to a slight dependence of η_0 on the frequency. The crossover is in principle given by the equality of (37) and (38) when $\Lambda_c'=l(L/l)^D$ or

$$\omega_c=[\sin(\eta_0\pi/2)/\sin(\eta_0\pi/2D)]^{D/(D-1)} \times(L^D\rho\gamma'/l^{D-1})^{-1/\eta_0}, \tag{39}$$

but the crossover frequency is difficult to determine with precision on the Bode plot itself.

EXTENSION TO $d=3$ ELECTRODES

If the electrode is a cylinder based on a self-similar fractal cross section of dimension D, its dimension is $D'=D+1$. If the height of the cylinder is L' its admittance would be $Y\approx LL'\rho^{\eta-1}(\gamma\omega)^{\eta}l^{\eta-1}$ with $\eta=1/(D'-1)$.

We show below that the circuit iteration procedure can be used in $d=3$ to generalize this formula. We consider now a fractal surface which is made in the following manner: a square (or a triangle) is cut in P equivalent smaller squares or triangles. In the same manner as in $d=2$, N parts are kept on the front and M are added. The fractal dimension of the surface is now

$$D=\ln(N+M)/\ln P^{1/2}. \tag{40}$$

If the smallest element of the 3D fractal electrode is a square of side l, it possesses an impedance

$$Z_0=(jl^2\gamma\omega)^{-1}. \tag{41}$$

Equation (5) is still valid, but from one stage to the next the electrolyte impedance R_n varies. R_0 is the resistance of a cube of side l, $R_0=\rho/l$, R_1 is the resistance of a cube of side $P^{1/2}l$, then $R_1=R_0/P^{1/2}$, and

$$R_n=R_0/P^{n/2}. \tag{42}$$

Using the reduced variables $z_n=Z_n/R_n$ the iteration equation (7) is now

$$\frac{P^{1/2}}{z_{n+1}}=\frac{N}{z_n+1}+\cfrac{P-N}{1+\cfrac{1}{\cfrac{m\beta}{z_n}+\cfrac{1}{\beta'+\cfrac{z_n}{M/(P-N)-m\beta}}}}, \tag{43}$$

where m represents the number of (vertical) walls of the pore. The reduced variable z_0 keeps the value given in (8). For the first stages of iteration relation (43) reduces to

$$z_{n+1}\approx P^{1/2}z_n/(N+M). \tag{44}$$

The critical value $n=\nu(\omega)$ for which $z_{\nu(\omega)}$ is of order 1 is now given by

$$z_{\nu(\omega)}\approx z_0P^{\nu(\omega)/2}(N+M)^{-\nu(\omega)}\approx 1 \tag{45}$$

and $\nu(\omega)$ is given by

$$\nu(\omega)\approx\ln|z_0|/\ln[(N+M)/P^{1/2}] =\ln(\Lambda/l)/\ln[(N+M)/P^{1/2}]. \tag{46}$$

After this stage we reach a regime in which $z_n<1$ and the iteration procedure (43) cannot be performed simply. In the case where $z_n<1$, (43) can be crudely approximated by using a first-order approximation:

$$z_{n+1}\approx P^{1/2}(1+z_n). \tag{47}$$

To obtain (47) we have postulated $\beta=1/m$ to ensure that the impedance of the total cell in that regime is inversely proportional to the size of the cell. Equation (47) shows that the reduced admittance $1/z_n$ of the cell is essentially real. Using a separation between the electrolyte and electrode contribution as in Eq. (13) we obtain for the limiting value of the electrolyte contribution, which is the principal term in (47),

$$z_{n=\infty,\text{yte}}\approx(P^{1/2}-1)^{-1}. \tag{48}$$

The electrode contribution to the cell impedance is obtained by replacing this value in (13) and (47)

$$z_{n+1,\text{ode}}\approx z_{n,\text{ode}}/P^{1/2}. \tag{49}$$

For an electrode of size L the iteration must be per-

formed $n(L)$ times such that

$$L = lP^{n(L)/2} . \tag{50}$$

The electrode impedance is given by

$$z_{n(L)} \approx P^{[\nu(\omega)-n(L)]/2} z_{\nu(\omega)} , \tag{51}$$

and using (41), (42), (46), (50), and (51) the result

$$Y \approx L^2 \rho^{\eta-1} (\gamma\omega)^{\eta} l^{\eta-1} \quad \text{with } \eta = 1/(D-1) \tag{52}$$

is obtained. The same result can be obtained through a crossover argument similar to that used in the $d=2$ case. For a given electrode, if the frequency is small enough, the response will be purely capacitive because $n(L) < \nu(\omega)$. The admittance is capacitive and

$$Y = l^2 (L/l)^D \gamma\omega . \tag{53}$$

On the contrary, if $n(L) > \nu(\omega)$, the admittance is of the CPA type. For a 3D electrode of size L the admittance must be proportional to L^{D_I} where D_I is the information dimension. From dimensional analysis the admittance must take the form

$$Y \approx L^{D_I} \rho^{\eta-1} (\gamma\omega)^{\eta} l^X \quad \text{with } D_I + X = \eta + 1 \tag{54}$$

because the only other length in the fractal is the smaller feature of size l. The crossover frequency ω_c is obtained when $n(L) = \nu(\omega_c)$ or from Eqs. (46) and (50)

$$\omega_c = (\rho\gamma l)^{-1} (L/l)^{1-D} . \tag{55}$$

At this crossover frequency both expressions (53) and (54) for Y must be equal and by equating the exponents of L the relationship

$$\eta = (D_I - 1)/(D-1) \tag{56}$$

is found. If the information dimension is equal to 2 in $d=3$, $\eta = 1/(D-1)$ as given by the iteration procedure in which $D_I = 2$ was assumed. In $d=3$ there could exist different values for D_I [39]. If we limit ourself to what could be called "corrugated" surfaces, which are "opaque," the value $D_I = 2$ holds most probably and $\eta = 1/(D-1)$.

In their early analysis of the response of ramified electrodes Sapoval and Chassaing claimed that the crossover frequency was approximately inversely proportional to the size of the electrode [40]. This fact is not compatible with Eq. (55) and the experimental results must be reexamined within the framework of this section. This will be published elsewhere.

The procedure described above (first the use of dimensional analysis, which constrains the power-law exponents in the fractal regime; second the use of the exact expression for the low-frequency impedance; and finally the matching of the high-frequency and the low-frequency impedance at the crossover frequency) is more general than described here. For the case of the Cantor bar electrodes or for the case of the modified Sierpinski electrodes one can find all the results of Refs. [12] and [15] by applying directly this method.

CONCLUSION

Because much confusion exists in this field, and for the sake of generality, we must discuss different (or apparently different) results. First, there exist fractal geometries which do not obey the same laws. It is the case of the Cantor bar and Sierpinski modified electrodes, but these electrodes are self-affine and not self-similar. In that case, there exist not two but three characteristic length scales: the large and small lateral cutoffs and a height parameter. Also the structure of the information fractal may be very different. In particular, for the "generalized modified Sierpinski electrode" the exponent is not a function of the fractal dimension only, but also of the aspect ratio of the pores [15].

For the case of connected spherical pores, Sapoval, Chazalviel, and Peyrière proposed [15] that the CPA exponent was not a function of the fractal dimension, but their calculation was valid only in the approximation in which the insertion of extra pores into a given pore would not change the capacitive surface of this pore. This does not apply to a true self-similar geometry. The case of dense 2D porous electrodes studied recently by Meakin and Sapoval corresponds also to a very different type of geometry [41].

In the case of a nonblocking surface, of macroscopic area S, described by a Faradaic resistance r the response (52) can be extended to

$$Y = S(\rho l)^{(2-D)/(D-1)} (r^{-1} + j\gamma\omega)^{1/(D-1)} . \tag{57}$$

The quantity $r^{-1} + j\gamma\omega$ represents the surface admittance. If the "flat" surface itself has a CPA response, $r^{-1} + j\gamma\omega$ should be replaced by $r^{-1} + \gamma'(j\omega)^{\eta_0}$ (where η_0 can be temperature dependent).

In summary, we have presented a comprehensive study of the response of singly connected self-similar electrodes. We have given four different approaches to this problem. The two theoretical approaches are a theory of scaling and an equivalent circuit iteration. Both these theories contains approximations. The scaling approach predicts "scaling relationships" where the prefactors are unknown but are expected to be of the order of unity. The iteration procedure is approximate in two ways: the equivalent circuit is a very simplified description of the real field in the cell and the iteration itself is approximated. Within these restrictions this calculation predicts a value for the impedance in which the prefactor is exactly one. The numerical simulations not only confirm the scaling forms but also indicate that the value of the prefactor is one within numerical uncertainty. This is an indication that the renormalization and coarse-graining procedure used here, although approximate, is an appropriate way to treat this problem. In this case the difference between the exact problem and its approximate version are not pertinent to the prediction of the real impedance for a self-similar geometry provided that we are far from the crossover. The experimental results are compatible with these

theories without any adjustable parameters. This may bring an end to a controversy on this question. The concept of information fractal may be developed to find the active zones that is those parts of the electrodes which are really "working" at a given frequency. This will be published elsewhere [38].

Finally, the same results should apply to transport across fractal membranes and to certain Eley-Rideal heterogeneous catalysis processes [5,6].

ACKNOWLEDGMENTS

The authors gratefully acknowledge useful discussions with M. Rosso, P. Jones, Th. Halsey, and J. Peyrière. This research was supported by NATO Grant No. CRG 900483. The Laboratoire de Physique de la Matière Condensée is "Unité de Recherche Associée du Centre National de la Recherche Scientifique No. 1254." The Laboratoire de Physique des Liquides et Electrochimie est laboratoire propre du CNRS No. 15.

[1] B. Mandelbrot, *The Fractal Geometry of Nature* (Freeman, San Francisco, 1982).
[2] B. Sapoval, *Fractals* (Aditech, Paris, 1990).
[3] G. H. Bell, D. Emslie-Smith, and C. R. Paterson, *Physiology and Biochemistry,* 9th ed. (Churchill Livinstone, Edimburgh, 1976).
[4] B. Sapoval, Acta Stereo. **6/III**, 785 (1987).
[5] B. Sapoval, in *Fractals and Disordered Systems,* edited by A. Bunde and S. Havlin (Springer-Verlag, Heidelberg, 1991), p. 207.
[6] B. Sapoval, C. R. Acad. Sci. Paris, Sér. 2, **312**, 599 (1991).
[7] W. Scheider, J. Phys. Chem. **79**, 127 (1975).
[8] R. D. Armstrong and R. A. Burnham, J. Electroanal. Chem. **72**, 257 (1976).
[9] I. Wolff, Phys. Rev. **27**, 755 (1926).
[10] J. R. Macdonald, Electrochim. Acta **35**, 1483 (1990), and references therein.
[11] A. Le Méhauté, Electrochim. Acta **34**, 591 (1989), and references therein.
[12] S. H. Liu, Phys. Rev. Lett. **55**, 529 (1985).
[13] L. Nyikos and T. Pajkossy, Electrochim. Acta **30**, 1533 (1985); Phys. Rev. B **42**, 709 (1990), and references therein.
[14] T. Kaplan, L. J. Gray, and S. H. Liu, Phys. Rev. B **35**, 5379 (1987), and references therein.
[15] B. Sapoval, J.-N. Chazalviel, and J. Peyrière, Phys. Rev. A **38**, 11 (1988); **38**, 5867 (1988), and references therein.
[16] R. M. Hill and L. A. Dissado, Solid State Ion. **26**, 295 (1988).
[17] R. Ball and M. Blunt, J. Phys. A **21**, 197 (1988).
[18] M. Blunt, J. Phys. A **21**, 179 (1989).
[19] Y. T. Chu, Solid State Ion. **26**, 299 (1988).
[20] R. de Levie, Electrochim. Acta **35**, 1045 (1990), and references therein.
[21] R. Blender, W. Dieterich, T. Kirchhoff, and B. Sapoval, J. Phys. A **23**, 1225 (1990).
[22] W. Geertsma, J. E. Gols, and L. Pietronero, Physica A **158**, 691 (1989).
[23] T. C. Halsey and M. Liebig, Europhys. Lett. **14**, 815 (1991); Phys. Rev. A **43**, 7087 (1991).
[24] M. Keddam and H. Takenouti, C. R. Acad. Sci. Paris, Sér. II **302**, 281 (1986); Electrochim. Acta. **33**, 445 (1988); and (unpublished).
[25] A. M. Marvin, F. Toigo, and A. Maritan, Surf. Sci. **211/212**, 422 (1989).
[26] W. H. Mulder and J. H. Sluyters, Electrochim. Acta **303**, 303 (1987).
[27] J. C. Wang, J. Electrochem. Soc. **134**, 1915 (1988); Solid State Ion. **28-30**, 133 (1988).
[28] J. B. Bates, Y. T. Chu, and W. T. Stribling, Phys. Rev. Lett. **60**, 627 (1988).
[29] D. L. Koch and A. S. Sangani, J. Electrochem. Soc. **137**, 475 (1991).
[30] G. L. M. K. S. Kahanda and M. Tomkiewicz, J. Electrochem. Soc. **137**, 3423 (1990).
[31] U. Rammelt and G. Reinhard, Electrochim. Acta **35**, 1045 (1990).
[32] B. Sapoval, J. Electrochem. Soc. **137**, 144C (1990).
[33] P. Meakin and B. Sapoval, Phys. Rev. A **43**, 2993 (1991).
[34] P. Jones and T. Wolff, Acta Math. **161**, 131 (1988).
[35] R. Ball, in *Surface Disordering, Growth, Roughening and Phase Transitions,* edited by R. Julien, P. Meakin, and D. Wolf (Nova Science, Commack, NY, 1993).
[36] C. J. Evertsz and B. B. Mandelbrot, J. Phys. A **25**, 1781 (1992).
[37] B. Sapoval (unpublished); B. Sapoval and R. Gutfraind, in *Surface Disordering, Growth, Roughening and Phase Transitions* (Ref. [35]), p. 285.
[38] R. Gutfraind and B. Sapoval, J. Phys. (Paris) I **3**, 1801 (1993).
[39] P. Jones (private communication).
[40] B. Sapoval and E. Chassaing, Physica A **157**, 610 (1989); E. Chassaing, B. Sapoval, G. Daccord, and R. Lenormand, J. Electroanal. Chem. **279**, 67 (1990).
[41] P. Meakin and B. Sapoval, Phys. Rev. A **46**, 1022 (1992).